

The molecular structure of the coherently superposed states of Malonaldehyde

Mohammad Goli¹ and Shant Shahbazian²

¹School of Nano Science, Institute for Research in Fundamental Sciences (IPM), Tehran
19395-5531, Iran,

Email: m_goli@ipm.ir

²Department of Physics, Shahid Beheshti University, Evin, Tehran, Iran,

E-mail: sh_shahbazian@sbu.ac.ir

Abstract

The proton between the two oxygen atoms of the malonaldehyde molecule experiences a double-well effective potential in which the one-proton wavefunction is delocalized between the two wells. Herein we employed the state-of-the-art multi-component quantum theory of atoms in molecules partitioning scheme to obtain the molecular structure, i.e. atoms in molecules and bonding network, from the malonaldehyde superposed ab initio wavefunctions. In contrast to the familiar clamped-proton portrayal of malonaldehyde, in which the proton forms a hydrogen basin, for the superposed states the hydrogen basin disappears and two novel hybrid oxygen-hydrogen basins appear instead, with an even distribution of the proton population between the two basins. The interaction between the hybrid basins is stabilizing thanks to an unprecedented mechanism involving the stabilizing classical Coulomb interaction of the proton one-density in one of the basins with the electron one-density in the other basin.

Keywords: Malonaldehyde; Atoms in Molecules; Quantum superposition, Molecular structure

The superposition principle is probably the most important principle of quantum mechanics with many theoretical ramifications like the exotic quantum correlations and the entanglement, which are quite intriguing from the classical physicist viewpoint.¹ In quantum chemistry and the electronic structure theory the superposition principle manifests itself by various linear combinations of atomic orbitals,² molecular orbitals,³ and Slater determinants.⁴ However, the majority of these manifestations include only the electronic states which are derived from the electronic Hamiltonian that treats electrons as quantum particles and nuclei as clamped point charges. Although it is generally highlighted that the electronic Hamiltonian is just an approximation based on the adiabatic separation of the electronic and nuclear motions,⁵ its almost-universal computational usage conceals its basic shortcoming, namely the total dismissal of the superposition of the nuclear states.⁶ To consider the superposed nuclear states, one may solve the nuclear Schrödinger equation using the potential energy surface (PES) derived from the solution of the electronic Schrödinger equation.⁷ However, this approach has rarely been used to challenge the viewpoint of the concept of “molecular structure” in which electrons are delocalized throughout the molecule while nuclei are conceived as point charges vibrating locally around their equilibrium positions.⁸ Some simple examples that may challenge this prototypical viewpoint are the inversion motion of pyramidal molecules, e.g. ammonia, and the inter-conversion of chiral isomers where both are usually modeled by an effective double-well potential.⁹ In these cases, there are two molecular structures each represented by a well and separated by a finite potential barrier; however, the true ground state wavefunction is indeed a superposition of the wavefunctions of these two structures.¹⁰ Evidently, in the superposed ground state certain, if not all, nuclei are “delocalized” in two

(or sometimes more) spatial positions, and the simple picture of a “localized” nucleus excusing around an equilibrium spatial point is no longer applicable. The question arises why such superposed states are not usually observable in chemical experiments. Various physical mechanisms, e.g. the environmentally induced decoherence,^{11,12} and certain mathematical constraints, e.g. the spontaneous symmetry breaking or the superselection rules,^{13,14} have been utilized to explain the subtlety of observation of such states. Nonetheless, currently, there is no doubt that it is experimentally feasible to construct such superposed states in a controllable way in sufficiently isolated situations.¹⁵

One interesting example of such systems is the malonaldehyde molecule wherein the proton between the two oxygen atoms experiences an effective double-well potential.¹⁶ The two indistinguishable conformers, depicted in Figure 1, are local minima on the PES, with C_s geometrical symmetry, that are derivable from the electronic Schrödinger equation.¹⁷ The proton transfer reaction involves a transition state, depicted in Figure 1, with C_{2v} geometrical symmetry.¹⁷

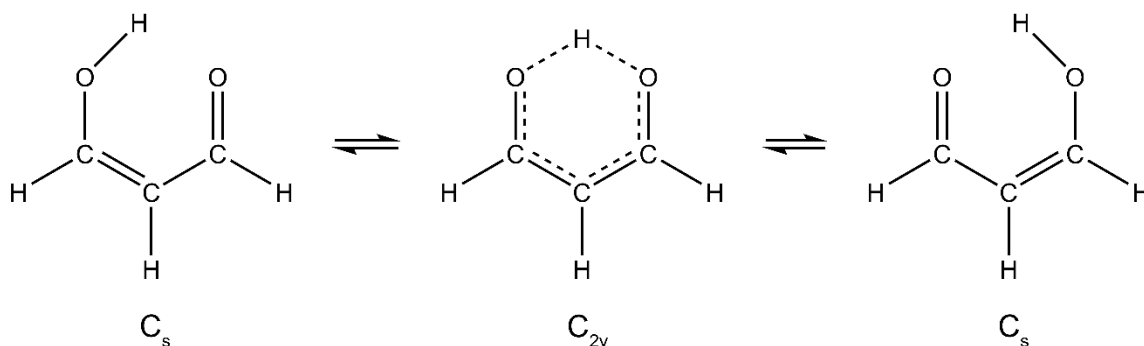


Figure 1 Schematic representation of the intra-molecular hydrogen transfer in malonaldehyde between the two conformers, C_s , passing through the transition state, C_{2v} .

The proton transfer between the two local minima may happen through the tunneling process, which has been extensively studied both theoretically and experimentally in the last decades (see the Supporting Information (SI) for a more comprehensive

bibliography).^{18–27} The tunneling mechanism implies that if Cs structures are prepared as the stationary states, an oscillatory time-dependent non-stationary process must transform one conformer to the other.¹⁶ The alternative “delocalized” scenario emerges if the proton is treated as a quantum particle from the outset of the ab initio calculations. The resulting two-component Hamiltonian, which contains the kinetic energy operators of the proton and electrons simultaneously, belongs to the realm of the multi-component (MC) quantum chemistry.^{28–31} In that case, the resulting two-component (TC) wavefunctions of the ground and first excited states contain the electronic and protonic variables concurrently. If the MC Schrödinger equation is solved with sufficient accuracy,^{32–34} the probability densities of the proton in both states reveal two peaks at two distinct positions between the two oxygen atoms. These superposed structures are depicted schematically as **4**, the ground state, and **5**, the first excited state, in Figure 2 and compared to structures **1** to **3**. In the latter structures, the quantum proton is automatically confined to a spatial excursion around a reference point at the minima or the maximum on the effective PES depicted in Figure 2, and in fact, these structures are the TC analogs of Cs and C_{2v}.

The molecular structures at their root are the networks of atoms in molecules (AIM) and their linking bonds. In line with this context, the quantum theory of atoms in molecules (QTAIM) is a quantum chemical partitioning methodology that divides a molecule exhaustively into atomic basins in the 3D real space and also partitions the molecular properties into the basin and inter-basin contributions.³⁵ Since the QTAIM partitioning algorithm solely employs the electronic wavefunctions as the inputs to derive AIM and their associated properties and interaction modes as the outputs, it fails to perform the AIM partitioning of the TC wavefunctions. To address this issue, an MC extension of the

QTAIM, called MC-QTAIM, has recently been developed that is capable of partitioning the MC quantum systems by employing the ab initio MC wavefunctions (see the SI for a brief overview of the machinery of the MC-QTAIM partitioning algorithm and the relevant references).^{36,37}

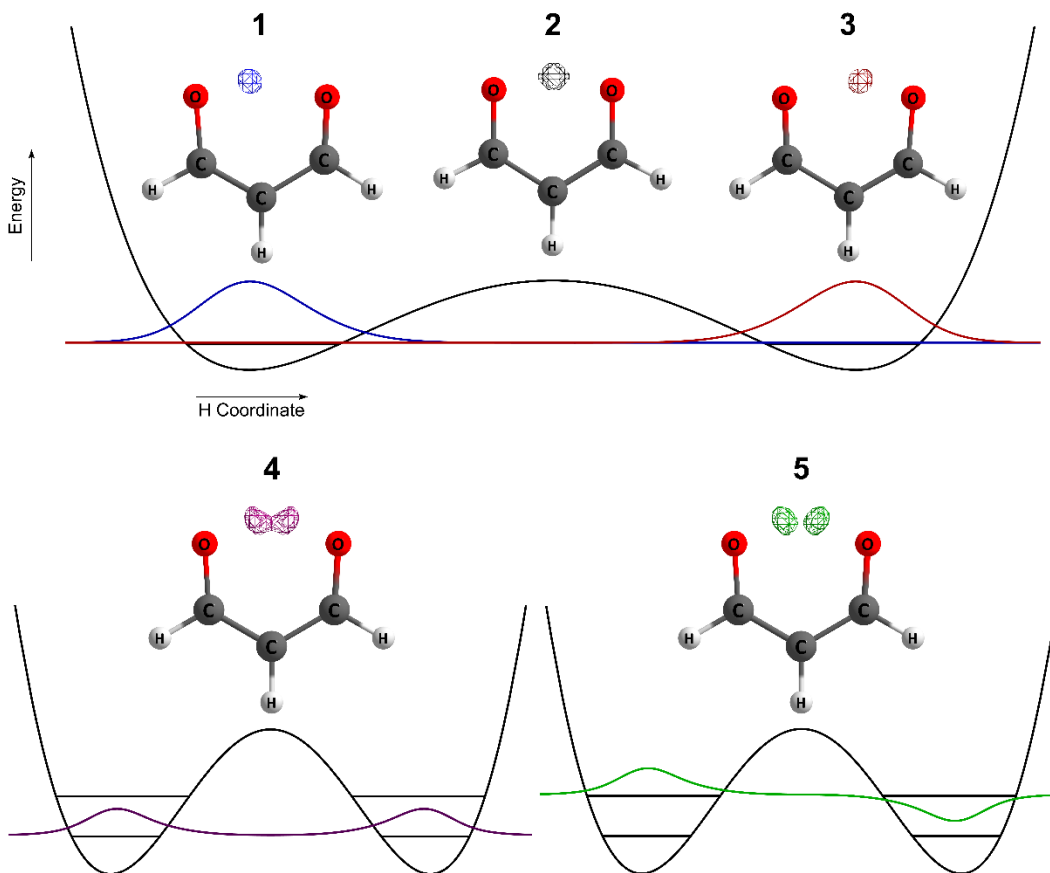


Figure 2 Schematic depictions of malonaldehyde structures with the localized (**1-3**) and delocalized protons (**4** and **5**), and, the corresponding potential energy surfaces and the one-proton wavefunctions.

Our goal in this study is to decipher the molecular structures of the superposed states of malonaldehyde, **4** and **5**, by applying the MC-QTAIM. To start the MC-QTAIM analysis, sufficiently-accurate MC wavefunctions of the superposed states of malonaldehyde were computed using the nuclear-electronic orbital density functional theory (NEO-DFT) which allows treating electrons and certain nuclei as quantum particles within the TC-DFT

framework.^{27,31,38,39} The computational details appendix contains the main steps of the procedure while a full description may be found in the extended computational details section in the SI. However, let us just stress that in the NEO-DFT, the TC-Kohn-Sham (KS) wavefunction is a product of the electronic Slater determinant and the protonic KS spin-orbital, and can be derived from the self-consistent field (SCF) solution of the TC-KS equations. The computed TC-KS wavefunctions are subsequently used to derive the one-electron, $\rho_1(\vec{r})$, and the one-proton, $\rho_2(\vec{r})$, densities as well as various energy partition terms (see the SI for more details). Figure 3 depicts the ab initio computed $\rho_2(\vec{r})$ revealing the expected “localized” nature of the proton density in **1** to **3** which is in marked contrast to its “delocalized” representation in **4** and **5**. At the next stage, the MC-QTAIM partitioning was performed by employing the Gamma density, $\Gamma^{(2)}(\vec{r}) = \rho_1(\vec{r}) + (1/m_{proton})\rho_2(\vec{r})$, and the results have been summarized in Figure 4. The topological analysis of $\vec{\nabla}\Gamma^{(2)}(\vec{r})$ in **1** to **3** yields the same number and types of critical points (CPs), and thus, provides the same types of AIM that were also previously deduced from the QTAIM analysis of the ab initio electronic wavefunction of **C_s** and **C_{2v}**.⁴⁰ In contrast, for the superposed states, **4** and **5**, the AIM structures are quite distinct and no hydrogen basin emerges between the two oxygen basins. It seems upon delocalization in two distinct spatial positions, the proton loses its capability to attract enough electrons and form its own maxima, i.e. (3, -3) CPs in $\Gamma^{(2)}(\vec{r})$, and somehow “dissolves” in the two basins containing the clamped oxygen nuclei. It seems that these exotic basins are better to be called the “hybrid oxygen-hydrogen” basins, hereafter denoted as *O4H* and *O5H*, to make a distinction from the usual oxygen basins in **1** to **3**.

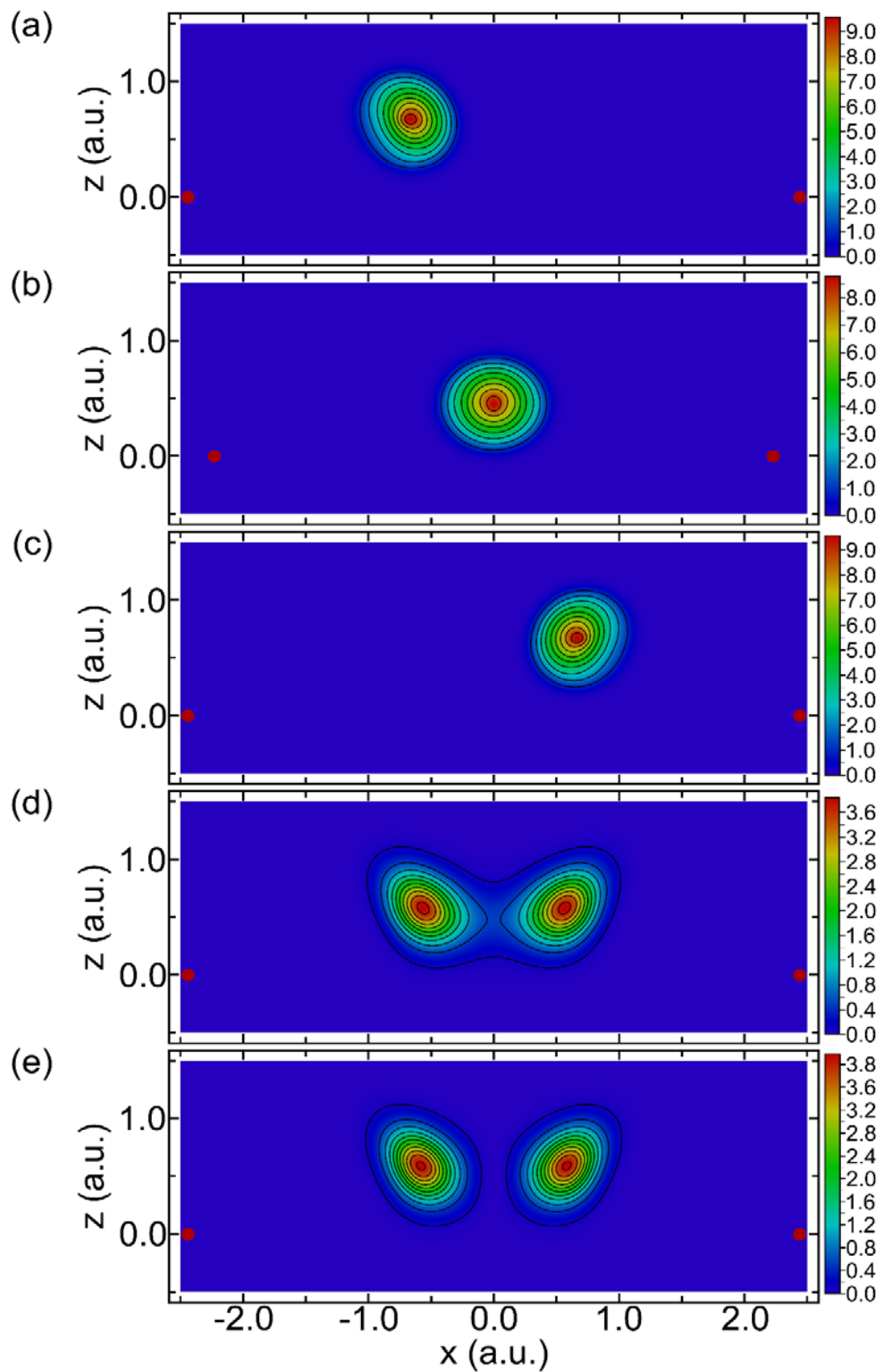


Figure 3 2D contour maps of the one-proton densities of (a) **1**, (b) **2**, (c) **3**, (d) **4** and (e) **5** structures. The positions of the clamped oxygen nuclei are depicted by red dots while the other nuclei are placed at the negative region of the z -axis on the xz plane (see Figure 1).

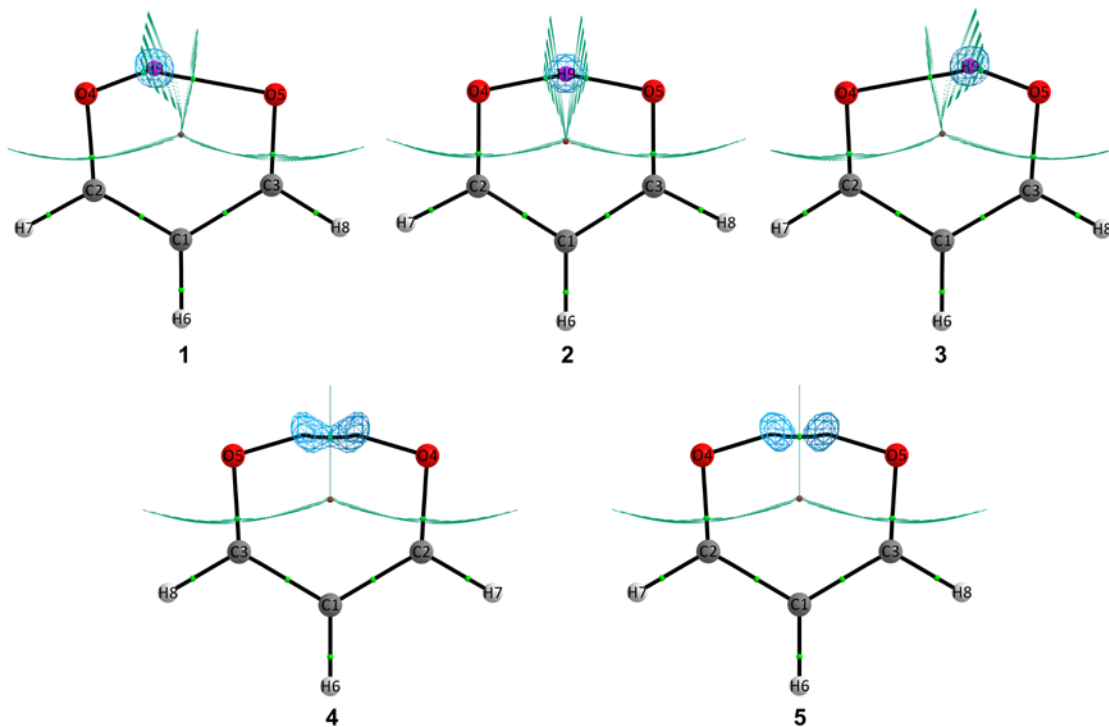


Figure 4 The AIM structures of **1** to **5**. In each structure, the blue spherical mesh is the 3D iso-density surface of the proton one-density shown at 0.0001 a.u. while the purple, red, and green spheres are the (3, -3), (3, +1), and (3, -1) CPs of $\Gamma^{(2)}(\vec{r})$, respectively. The black lines are the line paths and the green surfaces are the boundaries of the oxygen basins in **1** to **3** and the hybrid oxygen-hydrogen basins in **4** and **5**. The (3, -3) nuclear attractors at (or very near to) the clamped nuclei are shown by the larger spheres and labeled according to their elemental constituents.

In the previous studies, this phenomenon was observed only for the light positively-charged quantum particles, e.g. positrons.^{41,42} In such cases, the light particle resides in the atomic

basin of a clamped nucleus, and similarly in the present case, half of the proton's

population, $N_2(\Omega(O4H)) = N_2(\Omega(O5H)) = \int_{\Omega_{O4H}/\Omega_{O5H}} d\vec{r} \rho_2(\vec{r}) = 0.5$, resides in each of

the oxygen basins. Table 1 contains the atomic charges, $Q(A) = Z_\Omega - N_1(A) + N_2(A)$, of

basins and the electronic delocalization indices, $\delta_1(A, B)$,⁴³ between the neighboring

basins, i.e. those sharing an inter-atomic boundary, in **1** to **5**. The latter index is chemically

interpretable as a measure of the covalent bond order.⁴⁴ The numerical values of $\delta_1(A, B)$ imply the expected covalent networks of bonds in **1** to **3**, which are practically indistinguishable from those depicted in Figure 1. On the other hand, they reveal that the molecular structures of **4** and **5** are virtually the same, and the AIM structures and bonding networks of the backbones, i.e. all the basins except the two hybrid basins, as well as the bonding between the hybrid and neighboring carbon basins, are quite similar to that of **2**.

Table 1 The atomic charges and electronic delocalization index ($\delta_1(A, B)$) of species **1** to **5** (see Figure 4 for the numbering of the atomic basins).*

<i>Atomic basin</i>	3 (=1)	2	<i>Atomic basin</i>	3 (=1)	2
	<i>charge</i>	<i>charge</i>		$\delta_1(A, B)$	$\delta_1(A, B)$
C1	-0.02	-0.04			
C2	0.94	0.78	C1	1.14	1.32
C3	0.61	0.78	C1	1.51	1.32
O4	-1.14	-1.15	C2	1.34	1.19
O5	-1.20	-1.15	C3	1.05	1.19
H6	0.03	0.04	C1	0.96	0.97
H7	0.02	0.05	C2	0.90	0.91
H8	0.06	0.05	C3	0.92	0.91
H9	0.69	0.67	O5/O4	0.40/0.11	0.28
	4	5		4	5
C1	-0.05	-0.05			
C2	0.78	0.78	C1	1.32	1.32
C3	0.78	0.78	C1	1.32	1.32
H6	0.03	0.03	C1	0.97	0.97
H7	0.04	0.04	C2	0.91	0.91
H8	0.04	0.04	C3	0.91	0.91
O4H	-0.82	-0.82	C2	1.20	1.20
O5H	-0.82	-0.82	O4H	0.29	0.28

So, what remains unclear at this stage is the nature of the interaction between the hybrid basins. To dig into the nature of hybrid basins' interactions, the extended interacting quantum atoms (IQA) energy partitioning,^{42,45} was applied to **1** to **5**, and the computed two-particle inter-basin terms are considered herein (see the SI for the details and definition of

each term). The results of the extended IQA partitioning of **1** to **3**, gathered in Table 2, conform fully to the nature of bonds derived from the values of $\delta_1(A, B)$ and they may be used as the reference to deduce the nature of bonds in **4** and **5**.

Table 2 The selected results of the extended IQA energy partitioning for **1** to **3** (see Figure 4 for the numbering of the atomic basins).

		3 (=1)		
<i>Atomic basin</i>	<i>Atomic basin</i>	V_{elec}^{xc}	V_{elec}^{cl}	E_{inter}^{elec}
C1	C3	-0.446	0.064	-0.382
C2	C1	-0.352	0.049	-0.304
C3	O5	-0.316	-0.510	-0.826
H6	C1	-0.285	0.038	-0.247
H7	C2	-0.269	0.059	-0.211
H8	C3	-0.277	0.061	-0.216
O4	C2	-0.396	-0.722	-1.118
H9	O5	-0.127	0.159	0.032
H9	O4	-0.027	0.111	0.084
		2		
C1	C2/C3	-0.399	0.056	-0.343
C3	O5	-0.356	-0.612	-0.968
H6	C1	-0.287	0.038	-0.249
H7	C2	-0.274	0.063	-0.211
H8	C3	-0.274	0.063	-0.211
O4	C2	-0.356	-0.612	-0.968
H9	O5/O4	-0.084	0.154	0.069

Table 3 offers the results of the extended IQA analysis for **4** and **5** revealing the fact that they share quite similar bonding networks in the backbone. All the bonded basin pairs, except for the hybrid pair, have stabilizing inter-basin electronic interactions, $E_{inter}^{elec}(A, B) = V_{elec}^{cl}(A, B) + V_{elec}^{xc}(A, B)$, since the inter-basin electronic exchange-correlation interaction energies, $V_{elec}^{xc}(A, B)$, are always stabilizing. Adding the total inter-basin classical Coulomb interaction of electrons and clamped nuclei with the proton does

not change this picture and the total inter-basin interactions,

$E_{\text{inter}}^{\text{total}}(A, B) = E_{\text{inter}}^{\text{elec}}(A, B) + V_p^{\text{cl}}(A, B)$, are also always stabilizing.

Table 3 The selected results of the extended IQA energy partitioning for **4** and **5** (see Figure 4 for the numbering of the atomic basins).

4						
<i>Atomic basin</i>	<i>Atomic basin</i>	V_{ee}^{xc}	V_{elec}^{cl}	E_{inter}^{ee}	V_p^{cl}	$E_{\text{inter}}^{\text{total}}$
C1	C3	-0.398	0.053	-0.345	0.000	-0.345
C2	C1	-0.398	0.053	-0.345	0.000	-0.345
C3	O5	-0.358	-0.655	-1.013	0.145	-0.868
H6	C1	-0.286	0.037	-0.249	0.000	-0.249
H7	C2	-0.274	0.062	-0.212	0.000	-0.212
H8	C3	-0.274	0.062	-0.212	0.000	-0.212
O4H	C2	-0.358	-0.654	-1.012	0.145	-0.867
O5H	O4H	-0.055	0.425	0.370	-0.508	-0.138
5						
C1	C3	-0.398	0.053	-0.345	0.000	-0.345
C2	C1	-0.398	0.053	-0.345	0.000	-0.345
C3	O5	-0.358	-0.655	-1.013	0.147	-0.866
H6	C1	-0.286	0.037	-0.249	0.000	-0.249
H7	C2	-0.274	0.062	-0.212	0.000	-0.212
H8	C3	-0.274	0.062	-0.212	0.000	-0.212
O4H	C2	-0.358	-0.654	-1.012	0.147	-0.866
O5H	O4H	-0.053	0.423	0.370	-0.495	-0.124

In the case of the hybrid pair neither the inter-basin electronic exchange-correlation energy,

$V_{elec}^{xc}(\Omega_{O4H}, \Omega_{O5H})$, nor the inter-basin electronic classical Coulomb interaction energy,

$V_{elec}^{cl}(\Omega_{O4H}, \Omega_{O5H})$, are stabilizing interactions and the sole source of stabilizing interaction

is $V_p^{cl}(\Omega_{O4H}, \Omega_{O5H})$. The latter itself is composed of the destabilizing interaction between

the proton and the oxygen nuclei, $V_{pn}(\Omega_{O4H}, \Omega_{O5H}) + V_{pn}(\Omega_{O5H}, \Omega_{O4H})$, and the stabilizing

classical Coulomb interaction energy of the proton one-density in one of the basins with

the electron one-density in the other basin, $V_{ep}^{cl}(\Omega_{O4H}, \Omega_{O5H}) + V_{ep}^{cl}(\Omega_{O5H}, \Omega_{O4H})$. Thus, the very origin of the stabilizing interaction between the hybrid basins is the latter terms in $V_p^{cl}(\Omega_{O4H}, \Omega_{O5H})$, and it seems reasonable to claim that these terms yield an unconventional chemical bond between the two hybrid basins. Let us stress that this mechanism of bonding is unprecedented in usual molecules but it is interestingly quite similar to the mechanism of formation of the newly proposed “positronic bond”.^{42,46}

Malonaldehyde is usually conceived as a typical organic molecule with a molecular structure consisted of a network of well-known C-C, C-O, C-H and O-H covalent bonds, and an intra-molecular resonant-assisted hydrogen bond.⁴⁷ Even susceptibility to the tunneling mechanism does not change this picture profoundly and adds an extra dynamical, time-dependent, aspect to its molecular structure.⁴⁸ However as demonstrated in the present study, applying the superposition principle to the proton between the oxygen atoms alters significantly its molecular structure. In fact, the very basic and probably trivial idea that each atom is a node in the molecular graph is called into question in the superposed states, at least within the context of the present MC-QTAIM analysis. Evidently, a proper symbolic representation of molecular structures attributable to such exotic states is lacking in the current state of affairs and needs novel conventions and nomenclature. Probably, the fruitfulness of attributing molecular structures to such exotic states may be evaluated if they can be prepared experimentally and studied through various types of spectroscopic techniques. This may hopefully justify the proposed molecular structures, and in the next phase possibly lead to their “exotic chemistry”. Indeed, the analysis of the AIM structure and the bonding network of the superposed nuclear states is a completely uncharted

territory that awaits further theoretical and experimental developments and computational analysis.

Computational Methods

A thorough description of the used computational procedures as well as the relevant references may be found in the *extended Computational details* in the SI. Herein only a brief survey is done on the main procedures. The C_s and C_{2v} geometries of malonaldehyde, previously obtained by Hargis et al. at the CCSD(T)/cc-pVQZ level,¹⁷ were used for the geometry averaging procedure of the internal coordinates to deduce the backbone structure of the clamped nuclei in **4** and **5**. Then, the proton's wavefunction was derived from solving the 3D Schrödinger equation by the Numerov method in a cubic grid of 1.75 Å edge width, using 48 grid points per dimension.⁴⁹ In the next step, each numerical grid of the one-proton wavefunction was fitted to a set of 6s6p6d Gaussian functions, and this set was subsequently used as a fixed input in the NEO-DFT SCF procedure to yield the optimized electronic part of the TC-KS wavefunction at B3LYP/cc-pVTZ:6s6p6d level. The TC-KS wavefunctions of **1** to **3** were obtained at the two-component B3LYP:EPC17-1/cc-pVTZ:10s10p10d level.³⁹ The NEO methodology employed herein is part of our in-house version of the original NEO-GAMESS package.^{38,50} The AIMALL package, T. A. Keith, AIMAll (Version 13.11.04), TK Gristmill Software, Overland Park KS, USA, 2013, was used for the MC-QTAIM calculations including the graphics of the molecular graphs and the inter-atomic surfaces. All computational results are offered in the atomic units both in the main text and SI.

References

- ¹ M.P. Silverman, *Quantum Superposition* (Springer, 2008).
- ² T.A. Albright, J.K. Burdett, and M.-H. Whangbo, *Orbital Interactions in Chemistry*, 2nd edition (Wiley-Interscience, Hoboken, New Jersey, 2013).
- ³ I. Fleming, *Molecular Orbitals and Organic Chemical Reactions*, Student edition (Wiley, Chichester, West Sussex, U.K, 2009).
- ⁴ A. Szabo and N.S. Ostlund, *Modern Quantum Chemistry: Introduction to Advanced Electronic Structure Theory*, Reprint Edition (Dover Publications, Mineola, N.Y, 1996).
- ⁵ H. Moustroph, *ChemPhysChem* **17**, 2616 (2016).
- ⁶ B.T. Sutcliffe and R.G. Woolley, *Chem. Phys. Lett.* **408**, 445 (2005).
- ⁷ A.G. Császár, C. Fábri, T. Szidarovszky, E. Mátyus, T. Furtenbacher, and G. Czakó, *Phys. Chem. Chem. Phys.* **14**, 1085 (2012).
- ⁸ R.G. Woolley, *J. Chem. Educ.* **62**, 1082 (1985).
- ⁹ C. Presilla, G. Jona-Lasinio, and C. Toninelli, in *Multiscale Methods Quantum Mech.*, edited by P. Blanchard and G. Dell'Antonio (Birkhäuser, Boston, MA, 2004), pp. 119–127.
- ¹⁰ J.A. Cina and R.A. Harris, *Science* **267**, 832 (1995).
- ¹¹ M.A. Schlosshauer, *Decoherence and the Quantum-to-Classical Transition* (Springer, Berlin ; London, 2008).
- ¹² J. Trost and K. Hornberger, *Phys. Rev. Lett.* **103**, 023202 (2009).
- ¹³ U. Muller-Herold, *J. Chem. Educ.* **62**, 379 (1985).
- ¹⁴ C. Presilla and G. Jona-Lasinio, *Phys. Rev. A* **91**, 022709 (2015).
- ¹⁵ C. Monroe, D.M. Meekhof, B.E. King, and D.J. Wineland, *Science* **272**, 1131 (1996).
- ¹⁶ F. Fillaux and B. Nicolai, *Chem. Phys. Lett.* **415**, 357 (2005).
- ¹⁷ J.C. Hargis, F.A. Evangelista, J.B. Ingels, and H.F. Schaefer, *J. Am. Chem. Soc.* **130**, 17471 (2008).
- ¹⁸ M.E. Tuckerman and D. Marx, *Phys. Rev. Lett.* **86**, 4946 (2001).
- ¹⁹ M.D. Coutinho-Neto, A. Viel, and U. Manthe, *J. Chem. Phys.* **121**, 9207 (2004).
- ²⁰ R. Srinivasan, J.S. Feenstra, S.T. Park, S. Xu, and A.H. Zewail, *J. Am. Chem. Soc.* **126**, 2266 (2004).
- ²¹ C. Duan and D. Luckhaus, *Chem. Phys. Lett.* **391**, 129 (2004).
- ²² W. Caminati and J.-U. Grabow, *J. Am. Chem. Soc.* **128**, 854 (2006).
- ²³ T.N. Wassermann, D. Luckhaus, S. Coussan, and M.A. Suhm, *Phys. Chem. Chem. Phys.* **8**, 2344 (2006).
- ²⁴ Y. Wang, B.J. Braams, J.M. Bowman, S. Carter, and D.P. Tew, *J. Chem. Phys.* **128**, 224314 (2008).
- ²⁵ A. Hazra, J.H. Skone, and S. Hammes-Schiffer, *J. Chem. Phys.* **130**, 054108 (2009).
- ²⁶ W. Siebrand, Z. Smedarchina, and A. Fernández-Ramos, *J. Chem. Phys.* **139**, 021101 (2013).
- ²⁷ Z. Tao, Q. Yu, S. Roy, and S. Hammes-Schiffer, *Acc. Chem. Res.* **54**, 4131 (2021).
- ²⁸ H. Nakai, *Int. J. Quantum Chem.* **107**, 2849 (2007).
- ²⁹ T. Ishimoto, M. Tachikawa, and U. Nagashima, *Int. J. Quantum Chem.* **109**, 2677 (2018).
- ³⁰ A. Reyes, F. Moncada, and J. Charry, *Int. J. Quantum Chem.* **119**, e25705 (2019).
- ³¹ F. Pavošević, T. Culpitt, and S. Hammes-Schiffer, *Chem. Rev.* **120**, 4222 (2020).

- ³² M.V. Pak and S. Hammes-Schiffer, *Phys. Rev. Lett.* **92**, 103002 (2004).
- ³³ E. Kamarchik and D.A. Mazziotti, *Phys. Rev. A* **79**, 012502 (2009).
- ³⁴ Q. Yu and S. Hammes-Schiffer, *J. Phys. Chem. Lett.* **11**, 10106 (2020).
- ³⁵ R.F.W. Bader, *Atoms in Molecules: A Quantum Theory* (Clarendon Press, 1994).
- ³⁶ M. Goli and S. Shahbazian, *Theor. Chem. Acc.* **132**, 1365 (2013).
- ³⁷ M. Gharabaghi and S. Shahbazian, *J. Chem. Phys.* **146**, 154106 (2017).
- ³⁸ M.V. Pak, A. Chakraborty, and S. Hammes-Schiffer, *J. Phys. Chem. A* **111**, 4522 (2007).
- ³⁹ Y. Yang, K.R. Brorsen, T. Culpitt, M.V. Pak, and S. Hammes-Schiffer, *J. Chem. Phys.* **147**, 114113 (2017).
- ⁴⁰ P. Sanz, M.M. Montero-Campillo, O. M3, M. Y3ñez, I. Alkorta, and J. Elguero, *Theor. Chem. Acc.* **137**, 97 (2018).
- ⁴¹ M. Goli and S. Shahbazian, *Int. J. Quantum Chem.* **111**, 1982 (2011).
- ⁴² M. Goli and S. Shahbazian, *ChemPhysChem* **20**, 831 (2019).
- ⁴³ M. Goli and S. Shahbazian, *Theor. Chem. Acc.* **132**, 1410 (2013).
- ⁴⁴ C. Outeiral, M.A. Vincent, 3.M. Pend3s, and P.L.A. Popelier, *Chem. Sci.* **9**, 5517 (2018).
- ⁴⁵ M. Goli and S. Shahbazian, *ChemPhysChem* **17**, 3875 (2016).
- ⁴⁶ J. Charry, M.T. do N. Varella, and A. Reyes, *Angew. Chem. Int. Ed.* **57**, 8859 (2018).
- ⁴⁷ T. Steiner, *Angew. Chem. Int. Ed.* **41**, 48 (2002).
- ⁴⁸ H. Sekiya, in *At. Tunneling Phenom. Phys. Chem. Biol.*, edited by T. Miyazaki (Springer, Berlin, Heidelberg, 2004), pp. 201–231.
- ⁴⁹ U. Kuenzer, J.-A. Sorar3, and T.S. Hofer, *Phys. Chem. Chem. Phys.* **18**, 31521 (2016).
- ⁵⁰ M.W. Schmidt, K.K. Baldrige, J.A. Boatz, S.T. Elbert, M.S. Gordon, J.H. Jensen, S. Koseki, N. Matsunaga, K.A. Nguyen, S. Su, T.L. Windus, M. Dupuis, and J.A. Montgomery, *J. Comput. Chem.* **14**, 1347 (1993).

Supporting Information

The molecular structure of the coherently superposed states of Malonaldehyde

Mohammad Goli¹ and Shant Shahbazian²

¹School of Nano Science, Institute for Research in Fundamental Sciences (IPM), Tehran 19395-
5531, Iran,

Email: m_goli@ipm.ir

²Department of Physics, Shahid Beheshti University, Evin, Tehran, Iran

E-mail: sh_shahbazian@sbu.ac.ir

Table of contents

Pages 3-4: The extended list of references to theoretical and experimental studies of the tunneling process in malonaldehyde

Pages 5-9: A brief overview of the machinery of the MC-QTAIM

Pages 10-13: Extended computational details and references

Page 14: The optimized geometry of **1** (or **3**) and **2** at the CCSD(T)/cc-pVQZ level

Page 15: The averaged geometries of **4** and **5**

Pages 16-17: The regression procedure: Transforming numerical one-proton wavefunctions into Gaussian-type orbitals

Page 18: Table S1- Summary of the ab initio NEO-DFT results

The extended list of references to theoretical and experimental studies of the tunneling process in malonaldehyde

- [1] E.M. Fluder and J.R. De la Vega, *J. Am. Chem. Soc.* 100, 5265 (1978).
- [2] N. Shida, P.F. Barbara, and J.E. Almlöf, *J. Chem. Phys.* 91, 4061 (1989).
- [3] N. Shida, J. Almlöf, and P.F. Barbara, *J. Phys. Chem.* 95, 10457 (1991).
- [4] K. Luth and S. Scheiner, *J. Phys. Chem.* 98, 3582 (1994).
- [5] V.A. Benderskii, E.V. Vetoshkin, I.S. Irgibaeva, and H.-P. Trommsdorff, *Russ. Chem. Bull.* 50, 1148 (2001).
- [6] T.D. Sewell, Y. Guo, and D.L. Thompson, *J. Chem. Phys.* 103, 8557 (1995).
- [7] Z. Smedarchina, W. Siebrand, and M.Z. Zgierski, *J. Chem. Phys.* 103, 5326 (1995).
- [8] K. Wolf, W. Mikenda, E. Nusterer, and K. Schwarz, *J. Mol. Struct.* 448, 201 (1998).
- [9] M. Ben-Nun and T.J. Martínez, *J. Phys. Chem. A* 103, 6055 (1999).
- [10] V.A. Benderskii, E.V. Vetoshkin, I.S. Irgibaeva, and H.P. Trommsdorff, *Chem. Phys.* 262, 393 (2000).
- [11] M.E. Tuckerman and D. Marx, *Phys. Rev. Lett.* 86, 4946 (2001).
- [12] K. Yagi, T. Taketsugu, and K. Hirao, *J. Chem. Phys.* 115, 10647 (2001).
- [13] C.S. Tautermann, A.F. Voegelé, T. Loerting, and K.R. Liedl, *J. Chem. Phys.* 117, 1962 (2002).
- [14] D. Babić, S.D. Bosanac, and N. Došlić, *Chem. Phys. Lett.* 358, 337 (2002).
- [15] G.V. Mil'nikov, K. Yagi, T. Taketsugu, H. Nakamura, and K. Hirao, *J. Chem. Phys.* 119, 10 (2003).
- [16] G. Kovačević, T. Hrenar, and N. Došlić, *Chem. Phys.* 293, 41 (2003).
- [17] K. Yagi, G.V. Mil'nikov, T. Taketsugu, K. Hirao, and H. Nakamura, *Chem. Phys. Lett.* 397, 435 (2004).
- [18] M.D. Coutinho-Neto, A. Viel, and U. Manthe, *J. Chem. Phys.* 121, 9207 (2004).
- [19] K. Giese, M. Petković, H. Naundorf, and O. Kühn, *Phys. Rep.* 430, 211 (2006).
- [20] D.P. Tew, N.C. Handy, and S. Carter, *J. Chem. Phys.* 125, 084313 (2006).
- [21] A. Viel, M.D. Coutinho-Neto, and U. Manthe, *J. Chem. Phys.* 126, 024308 (2007).
- [22] P.P. Schmidt, *Mol. Phys.* 105, 1217 (2007).
- [23] Y. Wang, B.J. Braams, J.M. Bowman, S. Carter, and D.P. Tew, *J. Chem. Phys.* 128, 224314 (2008).
- [24] A. Hazra, J.H. Skone, and S. Hammes-Schiffer, *J. Chem. Phys.* 130, 054108 (2009).
- [25] M. Schröder, F. Gatti, and H.-D. Meyer, *J. Chem. Phys.* 134, 234307 (2011).
- [26] A. Yamada, H. Kojima, and S. Okazaki, *J. Chem. Phys.* 141, 084509 (2014).
- [27] U. Kuenzer, J.-A. Sorarù, and T.S. Hofer, *Phys. Chem. Chem. Phys.* 18, 31521 (2016).
- [28] Z. Tao, Q. Yu, S. Roy, and S. Hammes-Schiffer, *Acc. Chem. Res.* 54, 4131 (2021).

- [29] W.F. Rowe, R.W. Duerst, and E.B. Wilson, *J. Am. Chem. Soc.* 98, 4021 (1976).
- [30] R.S. Brown, *J. Am. Chem. Soc.* 99, 5497 (1977).
- [31] S.L. Baughcum, R.W. Duerst, W.F. Rowe, Z. Smith, and E.B. Wilson, *J. Am. Chem. Soc.* 103, 6296 (1981).
- [32] Z. Smith, E.B. Wilson, and R.W. Duerst, *Spectrochim. Acta Part Mol. Spectrosc.* 39, 1117 (1983).
- [33] S.L. Baughcum, Z. Smith, E.B. Wilson, and R.W. Duerst, *J. Am. Chem. Soc.* 106, 2260 (1984).
- [34] P. Turner, S.L. Baughcum, S.L. Coy, and Z. Smith, *J. Am. Chem. Soc.* 106, 2265 (1984).
- [35] G. Gilli, F. Bellucci, V. Ferretti, and V. Bertolasi, *J. Am. Chem. Soc.* 111, 1023 (1989).
- [36] D.W. Firth, K. Beyer, M.A. Dvorak, S.W. Reeve, A. Grushow, and K.R. Leopold, *J. Chem. Phys.* 94, 1812 (1991).
- [37] T. Chiavassa, P. Roubin, L. Pizzala, P. Verlaque, A. Allouche, and F. Marinelli, *J. Phys. Chem.* 96, 10659 (1992).
- [38] T. Baba, T. Tanaka, I. Morino, K.M.T. Yamada, and K. Tanaka, *J. Chem. Phys.* 110, 4131 (1999).
- [39] A.P. Cox, K.H. Hughes, and J.N. MacDonald, *Mol. Phys.* 101, 569 (2003).
- [40] A. Alparone and S. Millefiori, *Chem. Phys.* 290, 15 (2003).
- [41] R. Srinivasan, J.S. Feenstra, S.T. Park, S. Xu, and A.H. Zewail, *J. Am. Chem. Soc.* 126, 2266 (2004).
- [42] H. Sekiya, in *At. Tunneling Phenom. Phys. Chem. Biol.*, edited by T. Miyazaki (Springer, Berlin, Heidelberg, 2004), pp. 201–231.
- [42] C. Duan and D. Luckhaus, *Chem. Phys. Lett.* 391, 129 (2004).
- [43] Y. Arasaki, K. Yamazaki, M.T. do N. Varella, and K. Takatsuka, *Chem. Phys.* 311, 255 (2005).
- [44] R. Meyer and T.-K. Ha, *Mol. Phys.* 103, 2687 (2005).
- [45] W. Caminati and J.-U. Grabow, *J. Am. Chem. Soc.* 128, 854 (2006).
- [46] T.N. Wassermann, D. Luckhaus, S. Coussan, and M.A. Suhm, *Phys. Chem. Chem. Phys.* 8, 2344 (2006).
- [47] N.O.B. Lüttschwager, T.N. Wassermann, S. Coussan, and M.A. Suhm, *Mol. Phys.* 111, 2211 (2013).
- [48] W. Siebrand, Z. Smedarchina, and A. Fernández-Ramos, *J. Chem. Phys.* 139, 021101 (2013).
- [49] F. Fillaux and B. Nicolai, *Chem. Phys. Lett.* 415, 357 (2005).
- [50] F. Fillaux, A. Cousson, and M.J. Gutmann, *Pure Appl. Chem.* 79, 1023 (2007).
- [51] J. R. De La Vega, *Acc. Chem. Res.* 15, 185 (1982).
- [52] T. Carrington and W.H. Miller, *J. Chem. Phys.* 84, 4364 (1986).
- [53] J.C. Hargis, F.A. Evangelista, J.B. Ingels, and H.F. Schaefer, *J. Am. Chem. Soc.* 130, 17471 (2008).

A brief overview of the machinery of the MC-QTAIM

The QTAIM partitioning algorithm employs the electronic wavefunction, Ψ_e , as its input to exhaustively partition a molecule in the 3D real space into Q number of atomic basins, Ω_k , and divide molecular properties into the basin and inter-basin contributions.^[1] For an N -electron molecular system the boundaries of atomic basins are derivable from the local zero-flux equation of the electron density: $\vec{\nabla}\rho_e(\vec{r})\cdot\vec{n}(\vec{r})=0$ where: $\rho_e(\vec{r})=N\int d\vec{r}_2\dots\int d\vec{r}_N\sum_{spins}\Psi_e^*\Psi_e$. The boundaries are those zero-flux surfaces that are not crossing the nuclei and the unit vector normal to the surface, $\vec{n}(\vec{r})$, is perpendicular to the gradient of the electron density tangent to the surface.^[1] The contribution of each basin to the one-electron properties, $\hat{M}=\sum_{i=1}^N\hat{m}_i$, e.g. the kinetic

energy operator, is derivable from integrating the corresponding property density:

$$\langle\hat{M}\rangle=\sum_k^Q M_e(\Omega_k), \quad M_e(\Omega_k)=\int_{\Omega_k} d\vec{r} M_e(\vec{r}), \quad M_e(\vec{r})=N\int d\vec{r}_2\dots\int d\vec{r}_N\sum_{spins}\text{Re}[\Psi_e^*\hat{m}\Psi_e].^{[1]}$$
 For

two-electron properties, $\hat{G}=\sum_i^N\sum_{j>i}^N\hat{g}_{ij}$, e.g. the electron-electron interaction energy term, the

following recipe yields the basin and inter-basin contributions:

$$\langle\hat{G}\rangle=\sum_k^Q G(\Omega_k)+\sum_k^Q\sum_{l>k}^Q G(\Omega_k,\Omega_l),$$

$$G(\Omega_k)=(N(N-1)/2)\int_{\Omega_k} d\vec{r}_1\int_{\Omega_k} d\vec{r}_2\int d\vec{r}_3\dots\int d\vec{r}_N\sum_{spins}\text{Re}[\Psi_e^*\hat{g}(\vec{r}_1,\vec{r}_2)\Psi_e],$$

$$G(\Omega_k,\Omega_l)=N(N-1)\int_{\Omega_k} d\vec{r}_1\int_{\Omega_l} d\vec{r}_2\int d\vec{r}_3\dots\int d\vec{r}_N\sum_{spins}\text{Re}[\Psi_e^*\hat{g}(\vec{r}_1,\vec{r}_2)\Psi_e],$$
 which is particularly used

for the interacting quantum atoms (IQA) energy partitioning.^[2-6] The atomic basins are open to the exchange of electrons, and this is quantified through the introduction of the intra-basin variance

and inter-basin covariance of the electron number distribution within basins, which are generally non-zero quantities.^[1,7-12] The basin and inter-basin contributions are used to quantify the properties of AIM and their interaction modes, respectively, yielding the bonding network.^[1,13-17] Recently, the QTAIM scheme has been extended to the partitioning of the MC quantum systems, and the input to the extended algorithm, called MC-QTAIM,^[18-37] are ab initio MC wavefunctions derived from solving the MC Schrödinger equation (written in atomic units):

$$\begin{aligned} \hat{H}_{MC} \Psi_{MC} \left(\left\{ \bar{x}_{1,1}, \dots, \bar{x}_{1,N_1} \right\}, \dots, \left\{ \bar{x}_{s,1}, \dots, \bar{x}_{s,N_s} \right\}; \left\{ \bar{R}_\alpha \right\} \right) \\ = E_{MC} \left(\left\{ \bar{R}_\alpha \right\} \right) \Psi_{MC} \left(\left\{ \bar{x}_{1,1}, \dots, \bar{x}_{1,N_1} \right\}, \dots, \left\{ \bar{x}_{s,1}, \dots, \bar{x}_{s,N_s} \right\}; \left\{ \bar{R}_\alpha \right\} \right), \\ \hat{H}_{MC} = \sum_n^s (-1/2m_n) \sum_i^{N_n} \nabla_{n,i}^2 + \sum_n^s \sum_i^{N_n} \sum_{j>i}^{N_n} \frac{q_n^2}{|\bar{r}_{n,i} - \bar{r}_{n,j}|} + \sum_n^s \sum_{m>n}^s \sum_i^{N_n} \sum_j^{N_m} \frac{q_n q_m}{|\bar{r}_{n,i} - \bar{r}_{m,j}|} + \sum_n^s \sum_i^{N_n} \sum_\alpha^Q \frac{Z_\alpha q_n}{|\bar{R}_\alpha - \bar{r}_{n,i}|} \end{aligned}$$

This equation governs a system with s type of distinguishable quantum particles, with spin-spatial variables $\bar{x}_{n,i} = (\bar{r}_{n,i}, \sigma_{n,i})$, where each type contains N_n number of particles with charge, q_n , and mass, m_n , interacting via the Coulomb law with each other and the clamped nuclei; there are Q number of the latter carrying Z_α charge and placed at \bar{R}_α . The zero-flux equation of the MC-QTAIM partitioning algorithm, used to derive the boundaries of atomic basins, is as follows:^[25]

$$\bar{\nabla} \Gamma^{(s)}(\vec{r}) \cdot \vec{n}(\vec{r}) = 0, \quad \Gamma^{(s)}(\vec{r}) = \sum_n^s (m_1/m_n) \rho_n(\vec{r})$$

Wherein, $\rho_n(\vec{r}) = N_n \int d\bar{x}_{1,1} \dots \int d\bar{x}_{n-1,N_{n-1}} \int d\sigma_{n,1} \int d\bar{x}_{n,2} \dots \int d\bar{x}_{s,N_s} \Psi_{MC}^* \Psi_{MC}$ is the one-particle density of n -th type of particles.^[25] The Gamma density, $\Gamma^{(s)}$, which replaces the one-electron density used within the context of the QTAIM, is a mass-scaled combined density that includes the contributions of all quantum particles in shaping the boundaries. The numbering of particle types relies on their mass and starts from the lightest to the heaviest particle type, e.g. for a system

composed of electrons and protons as quantum particles, $\rho_1(\vec{r})$ and $\rho_2(\vec{r})$ are the electron and the proton one-densities, respectively. Some quantum particles, e.g. hydrogen isotopes, can form their own atomic basins, and the number of basins in an MC system is generally larger than the number of clamped nuclei, $P > Q$. The one-particle properties, $\hat{M} = \sum_n^s \hat{M}_n = \sum_n^s \left(\sum_i^{N_n} \hat{m}_{n,i} \right)$, are

partitioned into basin contributions as follows:^[24,25]

$$\langle \hat{M} \rangle = \left\langle \sum_n^s \sum_i^{N_n} \hat{m}_{n,i} \right\rangle = \sum_k^P \tilde{M}(\Omega_k), \quad \tilde{M}(\Omega_k) = \sum_n^s M_n(\Omega_k)$$

Wherein, $M_n(\Omega_k) = N_n \int d\vec{x}_{1,1} \dots \int d\vec{x}_{n-1,N_n} \int_{\Omega_k} d\vec{r}_{n,1} \int d\sigma_{n,1} \int d\vec{x}_{n,2} \dots \int d\vec{x}_{s,N_s} \text{Re} \left[\Psi_{MC}^* \hat{m}_{n,1} \Psi_{MC} \right]$ is the contribution of n -th type of particles to the basin property \hat{M} . In principle, the basin contribution originates from all types of particles though in practice some heavy particles are localized around a certain position and merely contribute to the properties of the basins within which they are confined.^[21,27–29,32] The partitioning of the two-particle properties,

$$\hat{G} = \sum_n^s \left(\sum_i^{N_n} \sum_{j>i}^{N_n} \hat{g}_{n,ij} \right) + \sum_n^s \sum_{m>n}^s \left(\sum_i^{N_n} \sum_j^{N_m} \hat{g}_{nm,ij} \right), \text{ is done as follows:}^{[32,35,36]}$$

$$\langle \hat{G} \rangle = \sum_k^P \tilde{G}(\Omega_k) + \sum_k^P \sum_{l>k}^P \tilde{G}(\Omega_k, \Omega_l),$$

$$\tilde{G}(\Omega_k) = \sum_n^s \left[G_n(\Omega_k) + \sum_{m>n}^s G_{nm}(\Omega_k) \right], \quad \tilde{G}(\Omega_k, \Omega_l) = \sum_n^s \left[G_n(\Omega_k, \Omega_l) + \sum_{m>n}^s G_{nm}(\Omega_k, \Omega_l) \right]$$

$$\text{Wherein: } G_n(\Omega_k) = (N_n(N_n - 1)/2) \int_{\Omega_k} d\vec{x}_{1,1} \dots \int d\vec{r}_{n,1} \int d\sigma_{n,1} \int_{\Omega_k} d\vec{r}_{n,2} \int d\sigma_{n,2} \dots \int d\vec{x}_{s,N_s} \text{Re} \left[\Psi_{MC}^* \hat{g}_n(\vec{r}_1, \vec{r}_2) \Psi_{MC} \right]$$

$$G_{nm}(\Omega_k) = N_n N_m \int_{\Omega_k} d\vec{x}_{1,1} \dots \int d\vec{r}_{n,1} \int d\sigma_{n,1} \dots \int_{\Omega_k} d\vec{r}_{m,1} \int d\sigma_{m,1} \dots \int d\vec{x}_{s,N_s} \text{Re} \left[\Psi_{MC}^* \hat{g}_{nm}(\vec{r}_{n,1}, \vec{r}_{m,1}) \Psi_{MC} \right],$$

$$G_n(\Omega_k, \Omega_l) = (N_n(N_n - 1)/2) \int_{\Omega_k} d\vec{x}_{1,1} \dots \int d\vec{r}_{n,1} \int d\sigma_{n,1} \int_{\Omega_l} d\vec{r}_{n,2} \int d\sigma_{n,2} \dots \int d\vec{x}_{s,N_s} \text{Re} \left[\Psi_{MC}^* \hat{g}_n(\vec{r}_1, \vec{r}_2) \Psi_{MC} \right],$$

$$G_{nm}(\Omega_k, \Omega_l) = N_n N_m \int_{\Omega_k} d\bar{x}_{1,1} \dots \int_{\Omega_k} d\bar{r}_{n,1} \int_{\Omega_l} d\sigma_{n,1} \dots \int_{\Omega_l} d\bar{r}_{m,1} \int_{\Omega_l} d\sigma_{m,1} \dots \int d\bar{x}_{s,N_s} \text{Re} \left[\Psi_{MC}^* \hat{g}_{nm}(\bar{r}_{n,1}, \bar{r}_{m,1}) \Psi_{MC} \right]. \quad \text{The}$$

prime application of this scheme is the extension of the IQA energy partitioning to the MC systems through the partitioning of the inter-particle Coulomb interactions, as recently detailed for the positronic systems.^[35]

The openness of atomic basins with respect to the electron exchange is quantified by introducing the basin particle number distributions, $P_m^n(\Omega_k)$, and then computing their mean, intra-basin variance and inter-basin covariance as follows:^[26,36]

$$P_m^n(\Omega_k) = \binom{N_n}{m} \int_{\Omega_k} d\bar{r}_{n,1} \dots \int_{\Omega_k} d\bar{r}_{n,m} \int_{R^3 - \Omega_k} d\bar{r}_{n,m+1} \dots \int_{R^3 - \Omega_k} d\bar{r}_{n,N_n} \prod_i^{N_n} \int d\sigma_{n,i} \int \bar{x}_{1,1} \dots \int d\bar{x}_{n-1,N_{n-1}} \int d\bar{x}_{n+1,1} \dots \int d\bar{x}_{s,N_s} \Psi_{MC}^* \Psi_{MC}$$

$$N_n(\Omega_k) = \sum_m^{N_n} m P_m^n(\Omega_k) = \int_{\Omega_k} d\bar{r} \rho_n(\bar{r}), \quad Cov_n(\Omega_k, \Omega_l) = \int_{\Omega_k} d\bar{r}_1 \int_{\Omega_l} d\bar{r}_2 \rho_n^{(2)}(\bar{r}_1, \bar{r}_2) - N_n(\Omega_k) N_n(\Omega_l)$$

$$Var_n(\Omega_k) = \sum_m^{N_n} (m - N(\Omega_k))^2 P_m^n(\Omega_k) = \int_{\Omega_k} d\bar{r}_1 \int_{\Omega_k} d\bar{r}_2 \rho_n^{(2)}(\bar{r}_1, \bar{r}_2) + N_n(\Omega_k) - [N_n(\Omega_k)]^2$$

Wherein, $\rho_n^{(2)}(\bar{r}_{n,1}, \bar{r}_{n,2}) = N_n(N_n - 1) \int d\bar{x}_{1,1} \dots \int d\bar{x}_{n-1,N_{n-1}} \int d\sigma_{n,1} \int d\sigma_{n,2} \int d\bar{x}_{n,3} \dots \int d\bar{x}_{s,N_s} \Psi_{MC}^* \Psi_{MC}$ is the spinless reduced second-order density matrix for the n -th type of particles.^[26,36] The basin particle number distribution is the probability distribution of observing m -particles from the n -th type within the k -th basin while the rest of $N_n - m$ particles are in the rest of the basins.

The index of particle delocalization is introduced as follows: $\delta_n(\Omega_k, \Omega_l) = 2|Cov_n(\Omega_k, \Omega_l)|$, which is the gauge of openness of an atomic basin with respect to the exchange of n -th type of particles with other basins.

The inter-basin terms of the extended IQA partitioning for a two-component (TC) system composed of electrons and a proton are as follows:

$$V_{elec}^{cl}(\Omega_k, \Omega_l) = V_{en}(\Omega_k, \Omega_l) + V_{en}(\Omega_l, \Omega_k) + V_{ee}^{cl}(\Omega_k, \Omega_l) + V_{nn}(\Omega_k, \Omega_l)$$

$$V_p^{cl}(\Omega_k, \Omega_l) = V_{ep}^{cl}(\Omega_k, \Omega_l) + V_{ep}^{cl}(\Omega_l, \Omega_k) + V_{pn}(\Omega_k, \Omega_l) + V_{pn}(\Omega_l, \Omega_k)$$

$$E_{inter}^{elec}(\Omega_k, \Omega_l) = V_{elec}^{cl}(\Omega_k, \Omega_l) + V_{elec}^{xc}(\Omega_k, \Omega_l)$$

$$E_{inter}^{total}(\Omega_k, \Omega_l) = E_{inter}^{elec}(\Omega_k, \Omega_l) + V_p^{cl}(\Omega_k, \Omega_l) + V_{ep}^c(\Omega_k, \Omega_l) + V_{ep}^c(\Omega_l, \Omega_k)$$

Wherein:

$$V_{en}(\Omega_k, \Omega_l) = -Z_k \int_{\Omega_l} d\vec{r}_{1,1} \frac{\rho_1(\vec{r}_{1,1})}{|\vec{r}_{1,1} - \vec{R}_k|}, \quad V_{en}(\Omega_l, \Omega_k) = -Z_l \int_{\Omega_k} d\vec{r}_{1,1} \frac{\rho_1(\vec{r}_{1,1})}{|\vec{r}_{1,1} - \vec{R}_l|},$$

$$V_{ee}^{cl}(\Omega_k, \Omega_l) = \int_{\Omega_k} d\vec{r}_{1,1} \int_{\Omega_l} d\vec{r}_{1,2} \frac{\rho_1(\vec{r}_{1,1}) \rho_1(\vec{r}_{1,2})}{|\vec{r}_{1,1} - \vec{r}_{1,2}|}, \quad V_{elec}^{xc}(\Omega_k, \Omega_l) = \int_{\Omega_k} d\vec{r}_{1,1} \int_{\Omega_l} d\vec{r}_{1,2} \frac{\rho_1^{xc}(\vec{r}_{1,1}, \vec{r}_{1,2})}{|\vec{r}_{1,1} - \vec{r}_{1,2}|}$$

$$V_{nn}(\Omega_k, \Omega_l) = \frac{Z_k Z_l}{|\vec{R}_k - \vec{R}_l|}, \quad V_{ep}^{cl}(\Omega_k, \Omega_l) = - \int_{\Omega_k} d\vec{r}_{1,1} \int_{\Omega_l} d\vec{r}_{2,1} \frac{\rho_1(\vec{r}_{1,1}) \rho_2(\vec{r}_{2,1})}{|\vec{r}_{1,1} - \vec{r}_{2,1}|}$$

$$V_{ep}^{cl}(\Omega_l, \Omega_k) = - \int_{\Omega_l} d\vec{r}_{1,1} \int_{\Omega_k} d\vec{r}_{2,1} \frac{\rho_1(\vec{r}_{1,1}) \rho_2(\vec{r}_{2,1})}{|\vec{r}_{1,1} - \vec{r}_{2,1}|}, \quad V_{pn}(\Omega_k, \Omega_l) = Z_k \int_{\Omega_l} d\vec{r}_{2,1} \frac{\rho_2(\vec{r}_{2,1})}{|\vec{r}_{2,1} - \vec{R}_k|},$$

$$V_{pn}(\Omega_l, \Omega_k) = Z_l \int_{\Omega_l} d\vec{r}_{2,1} \frac{\rho_2(\vec{r}_{2,1})}{|\vec{r}_{2,1} - \vec{R}_l|}, \quad V_{ep}^c(\Omega_k, \Omega_l) = - \int_{\Omega_l} d\vec{r}_{1,1} \int_{\Omega_k} d\vec{r}_{2,1} \frac{\rho_{12}^c(\vec{r}_{1,1}, \vec{r}_{2,1})}{|\vec{r}_{1,1} - \vec{r}_{2,1}|},$$

$$V_{ep}^c(\Omega_k, \Omega_l) = - \int_{\Omega_l} d\vec{r}_{1,1} \int_{\Omega_k} d\vec{r}_{2,1} \frac{\rho_{12}^c(\vec{r}_{1,1}, \vec{r}_{2,1})}{|\vec{r}_{1,1} - \vec{r}_{2,1}|}$$

In this partitioning scheme the spinless reduced second-order density matrix for electrons and the electron-proton pair density are decomposed as follows:

$$\rho_1^{(2)}(\vec{r}_{1,1}, \vec{r}_{1,2}) = \rho_1(\vec{r}_{1,1}) \rho_1(\vec{r}_{1,2}) + \rho_{xc}(\vec{r}_{1,1}, \vec{r}_{1,2}), \quad \rho_{12}^{(2)}(\vec{r}_{1,1}, \vec{r}_{2,1}) = \rho_1(\vec{r}_{1,1}) \rho_2(\vec{r}_{2,1}) + \rho_{12}^c(\vec{r}_{1,1}, \vec{r}_{2,1}),$$

respectively, where the pair density is defined as follows:

$$\rho_{12}^{(2)}(\vec{r}_{1,1}, \vec{r}_{2,1}) = N_1 N_2 \int d\sigma_{1,1} \int d\vec{x}_{1,2} \dots \int d\vec{x}_{1,N_1} \int d\sigma_{2,1} \int d\vec{x}_{2,2} \dots \int d\vec{x}_{2,N_2} \Psi_{TC}^* \Psi_{TC}.$$

Extended Computational details

The computational implementation of the NEO-DFT includes the SCF solution of TC-KS equations using the KS potentials derived from the electron-electron and electron-proton functionals.^[38–45] In principle, if the proper electron-electron exchange-correlation functional and the electron-proton correlation functional are employed, through simultaneous optimization of the geometry of clamped nuclei and the one-electron and the one-proton densities, the superposed states of malonaldehyde must be recovered. However, many studies revealed that this is not an achievable task with the currently available electron-proton correlation functionals.^[46–49] In fact, full optimization through TC-KS equations as detailed above, yields “broken symmetry” KS wavefunctions that are basically describing structures **1** and **3**. Even more, in the whole toolkit of the ab initio MC quantum chemistry, only very accurate MC-full-configuration-interaction derived wavefunctions, or very high-quality MC-multi-configurational SCF wavefunctions, may recover the delocalized states via full optimization.^[47] Such methodologies are beyond the current computational capacity for systems with a size around malonaldehyde, and inevitably some computational tricks like the “geometry/state-averaging” must be used to reach the desired “delocalized” KS wavefunctions.^[50,51] Accordingly, in the first step, a geometry for clamped nuclei in **4** and **5** was generated by the geometry-averaging method of the internal coordinates of the equilibrium geometries of **1** and **3**, deduced at CCSD(T)/cc-pVQZ level (see pages 14 and 15).^[52] In the averaging procedure, the arithmetic mean of the corresponding Z-matrix coordinates of **1** and **3** was computed after ordering the coordinates of the two Z-matrices. To obtain the ground and first excited one-proton wavefunctions in **4** and **5**, respectively, the three-dimensional time-independent Schrödinger equation of the quantum proton was solved by the Numerov method, the used proton mass is 1836.153 in atomic units, in a cubic grid of 1.75 Å edge width, using 48 grid

points per dimension based on the averaged geometries for clamped nuclei.^[53] The corresponding electronic ground-state PES for the Numerov method was derived at MP2/cc-pVTZ level at each grid point assuming a clamped proton. The high efficiency and accuracy of the *improved* Numerov method in solving high dimensional differential equations have been recently demonstrated in considering the molecular vibrational modes.^[54–56] In the present study, we used the 7-point stencil that enabled us to reach the accuracy $O(10^{-7})$ in the solution of the grid-based Numerov methodology. In addition, the JADAMILU eigenvalue problem library was employed for the diagonalization procedure that takes advantage of the highly-sparse representation of the Hamiltonian formed within the Numerov approach.^[57] Subsequently, each 3D grid of the resulting one-proton wavefunctions was fitted to a set of [6s6p6d] Gaussian basis functions by simultaneous optimization of their coefficients, exponents and centers (see pages 16 and 17 for details). Subsequently, the derived protonic wavefunction was kept fixed and used as the protonic KS orbital in the NEO-DFT SCF procedure to yield the optimized electronic part of the TC-KS wavefunction at B3LYP/[cc-pVTZ:6s6p6d] level.^[58,59] Instead of the usual single-center expansion of the electronic basis functions, two sets of cc-pVTZ basis set were placed at the two positions corresponding to the maxima of the one-proton densities depicted in Figure 3. At the next stage, and for comparison purposes, the TC-KS wavefunctions for **1** to **3**, were obtained by using the CCSD(T)/cc-pVQZ optimized geometries.^[52] The protonic KS spatial orbital in each of the structures **1** to **3** was expanded by [10s10p10d] uncontracted shells of even-tempered Gaussian basis functions, which are placed at the optimized position of the transferring proton and their exponents spanned the range of $2\sqrt{2}$ to 64. In addition, the cc-pVTZ basis set was used to expand the electronic KS orbitals employing the clamped proton position derived at the CCSD(T)/cc-pVQZ level as the center of the electronic basis set. The used even-tempered protonic basis set is

flexible enough to capture the anharmonicity and anisotropy of the protonic orbital, as has been shown in several recent NEO-DFT studies.^[44,60] The recently developed EPC17-1 electron-proton correlation functional was used to produce high-quality protonic orbitals that are comparable to highly accurate ab-initio results of the MC coupled-cluster theory.^[43,61] The NEO methodology was originally implemented into the GAMESS quantum chemistry package although the computations reported in the present account were derived via our in-house version of the NEO-GAMESS package.^[46,40,62] Some details of the ab initio results are gathered in Table S1 on page 18. The extended IQA partitioning of the electronic exchange-correlation energy of **1** to **5** was done according to the formalism developed previously for the IQA-DFT partitioning.^[63,64] Since no electron-proton correlation functional is used in the NEO-DFT calculations of **4** and **5**, the electron-proton correlation energy is zero and the total inter-basin interaction energy reduces:

$$E_{\text{inter}}^{\text{total}}(\Omega_k, \Omega_l) = E_{\text{inter}}^{\text{elec}}(\Omega_k, \Omega_l) + V_p^{\text{cl}}(\Omega_k, \Omega_l).$$

References

- [1] R. F. W. Bader, *Atoms in Molecules: A Quantum Theory*, Clarendon Press, **1994**.
- [2] P. L. A. Popelier, D. S. Kosov, *J. Chem. Phys.* **2001**, *114*, 6539–6547.
- [3] M. A. Blanco, A. Martín Pendás, E. Francisco, *J. Chem. Theory Comput.* **2005**, *1*, 1096–1109.
- [4] E. Francisco, A. Martín Pendás, M. A. Blanco, *J. Chem. Theory Comput.* **2006**, *2*, 90–102.
- [5] J. M. Guevara-Vela, E. Francisco, T. Rocha-Rinza, Á. Martín Pendás, *Molecules* **2020**, *25*, 4028.
- [6] A. F. Silva, L. J. Duarte, P. L. A. Popelier, *Struct. Chem.* **2020**, *31*, 507–519.
- [7] R. F. W. Bader, M. E. Stephens, *Chem. Phys. Lett.* **1974**, *26*, 445–449.
- [8] R. F. W. Bader, M. E. Stephens, *J. Am. Chem. Soc.* **1975**, *97*, 7391–7399.
- [9] X. Fradera, M. A. Austen, R. F. W. Bader, *J. Phys. Chem. A* **1999**, *103*, 304–314.
- [10] X. Fradera, J. Poater, S. Simon, M. Duran, M. Solà, *Theor. Chem. Acc.* **2002**, *108*, 214–224.
- [11] E. Francisco, A. Martín Pendás, M. A. Blanco, *J. Chem. Phys.* **2007**, *126*, 094102.
- [12] Á. M. Pendás, E. Francisco, *ChemPhysChem* **2019**, *20*, 2722–2741.
- [13] P. L. Popelier, *Atoms in Molecules: An Introduction*, Prentice Hall, Harlow, **2000**.
- [14] C. F. Matta, R. J. Boyd, *The Quantum Theory of Atoms in Molecules: From Solid State to DNA and Drug Design*, Wiley-VCH, Weinheim, **2007**.
- [15] M. García-Revilla, E. Francisco, P. L. A. Popelier, A. M. Pendás, *ChemPhysChem* **2013**, *14*, 1211–1218.
- [16] C. F. Matta, *Comput. Theor. Chem.* **2018**, *1124*, 1–14.
- [17] C. Outeiral, M. A. Vincent, Á. M. Pendás, P. L. A. Popelier, *Chem. Sci.* **2018**, *9*, 5517–5529.
- [18] P. Nasertayoob, M. Goli, S. Shahbazian, *Int. J. Quantum Chem.* **2011**, *111*, 1970–1981.
- [19] M. Goli, S. Shahbazian, *Int. J. Quantum Chem.* **2011**, *111*, 1982–1998.

- [20] F. Heidar Zadeh, S. Shahbazian, *Int. J. Quantum Chem.* **2011**, *111*, 1999–2013.
- [21] M. Goli, S. Shahbazian, *Theor. Chem. Acc.* **2011**, *129*, 235–245.
- [22] M. Goli, S. Shahbazian, *Theor. Chem. Acc.* **2012**, *131*, 1208.
- [23] S. Shahbazian, *Found. Chem.* **2013**, *15*, 287–302.
- [24] M. Goli, S. Shahbazian, *Theor. Chem. Acc.* **2013**, *132*, 1362.
- [25] M. Goli, S. Shahbazian, *Theor. Chem. Acc.* **2013**, *132*, 1365.
- [26] M. Goli, S. Shahbazian, *Theor. Chem. Acc.* **2013**, *132*, 1410.
- [27] M. Goli, S. Shahbazian, *Phys. Chem. Chem. Phys.* **2014**, *16*, 6602–6613.
- [28] M. Goli, S. Shahbazian, *Comput. Theor. Chem.* **2015**, *1053*, 96–105.
- [29] M. Goli, S. Shahbazian, *Phys. Chem. Chem. Phys.* **2015**, *17*, 245–255.
- [30] M. Goli, S. Shahbazian, *Phys. Chem. Chem. Phys.* **2015**, *17*, 7023–7037.
- [31] M. Goli, S. Shahbazian, *Chem. - Eur. J.* **2016**, *22*, 2525–2531.
- [32] M. Goli, S. Shahbazian, *ChemPhysChem* **2016**, *17*, 3875–3880.
- [33] M. Gharabaghi, S. Shahbazian, *J. Chem. Phys.* **2017**, *146*, 154106.
- [34] M. Goli, S. Shahbazian, *Phys. Chem. Chem. Phys.* **2018**, *20*, 16749–16760.
- [35] M. Goli, S. Shahbazian, *ChemPhysChem* **2019**, *20*, 831–837.
- [36] S. Shahbazian, *arXiv:2109.15008* **2021**.
- [37] S. Shahbazian, *arXiv:2204.09604* **2022**.
- [38] Z. Tao, Q. Yu, S. Roy, S. Hammes-Schiffer, *Acc. Chem. Res.* **2021**, *54*, 4131–4141.
- [39] F. Pavošević, T. Culpitt, S. Hammes-Schiffer, *Chem. Rev.* **2020**, *120*, 4222–4253.
- [40] M. V. Pak, A. Chakraborty, S. Hammes-Schiffer, *J. Phys. Chem. A* **2007**, *111*, 4522–4526.
- [41] A. Chakraborty, M. V. Pak, S. Hammes-Schiffer, *Phys. Rev. Lett.* **2008**, *101*, 153001.
- [42] K. R. Brorsen, Y. Yang, S. Hammes-Schiffer, *J. Phys. Chem. Lett.* **2017**, *8*, 3488–3493.
- [43] Y. Yang, K. R. Brorsen, T. Culpitt, M. V. Pak, S. Hammes-Schiffer, *J. Chem. Phys.* **2017**, *147*, 114113.
- [44] K. R. Brorsen, P. E. Schneider, S. Hammes-Schiffer, *J. Chem. Phys.* **2018**, *149*, 044110.
- [45] Z. Tao, Y. Yang, S. Hammes-Schiffer, *J. Chem. Phys.* **2019**, *151*, 124102.
- [46] S. P. Webb, T. Jordanov, S. Hammes-Schiffer, *J. Chem. Phys.* **2002**, *117*, 4106–4118.
- [47] M. V. Pak, S. Hammes-Schiffer, *Phys. Rev. Lett.* **2004**, *92*, 103002.
- [48] M. V. Pak, C. Swalina, S. P. Webb, S. Hammes-Schiffer, *Chem. Phys.* **2004**, *304*, 227–236.
- [49] E. Kamarchik, D. A. Mazziotti, *Phys. Rev. A* **2009**, *79*, 012502.
- [50] A. Hazra, J. H. Skone, S. Hammes-Schiffer, *J. Chem. Phys.* **2009**, *130*, 054108.
- [51] Q. Yu, S. Hammes-Schiffer, *J. Phys. Chem. Lett.* **2020**, *11*, 10106–10113.
- [52] J. C. Hargis, F. A. Evangelista, J. B. Ingels, H. F. Schaefer, *J. Am. Chem. Soc.* **2008**, *130*, 17471–17478.
- [53] U. Kuenzer, J.-A. Sorarù, T. S. Hofer, *Phys. Chem. Chem. Phys.* **2016**, *18*, 31521–31533.
- [54] U. Kuenzer, M. Klotz, T. S. Hofer, *J. Comput. Chem.* **2018**, *39*, 2196–2209.
- [55] U. Kuenzer, T. S. Hofer, *Chem. Phys.* **2019**, *520*, 88–99.
- [56] M. J. Schuler, T. S. Hofer, Y. Morisawa, Y. Futami, C. W. Huck, Y. Ozaki, *Phys. Chem. Chem. Phys.* **2020**, *22*, 13017–13029.
- [57] M. Bollhöfer, Y. Notay, *Comput. Phys. Commun.* **2007**, *177*, 951–964.
- [58] T. H. Dunning, *J. Chem. Phys.* **1989**, *90*, 1007–1023.
- [59] A. D. Becke, *J. Chem. Phys.* **1993**, *98*, 5648–5652.
- [60] Y. Yang, T. Culpitt, Z. Tao, S. Hammes-Schiffer, *J. Chem. Phys.* **2018**, *149*, 084105.
- [61] F. Pavošević, T. Culpitt, S. Hammes-Schiffer, *J. Chem. Theory Comput.* **2019**, *15*, 338–347.
- [62] M. W. Schmidt, K. K. Baldridge, J. A. Boatz, S. T. Elbert, M. S. Gordon, J. H. Jensen, S. Koseki, N. Matsunaga, K. A. Nguyen, S. Su, T. L. Windus, M. Dupuis, J. A. Montgomery, *J. Comput. Chem.* **1993**, *14*, 1347–1363.
- [63] P. Maxwell, Á. M. Pendás, P. L. A. Popelier, *Phys. Chem. Chem. Phys.* **2016**, *18*, 20986–21000.
- [64] E. Francisco, J. L. Casals-Sainz, T. Rocha-Rinza, A. Martín Pendás, *Theor. Chem. Acc.* **2016**, *135*, 170.

The optimized geometry of 1 (or 3) at the CCSD(T)/cc-pVQZ level				
Atom	Number	Coordinates [Bohr]		
		X	Y	Z
C	1	0.000000	2.077361	0.000000
C	2	2.339522	0.675322	0.000000
C	3	-2.236791	0.811101	0.000000
O	4	2.439903	-1.657362	0.000000
O	5	-2.441842	-1.681011	0.000000
H	6	0.019948	4.116154	0.000000
H	7	4.109976	1.763188	0.000000
H	8	-4.041823	1.778489	0.000000
H*	9	-0.688985	-2.333555	0.000000

* The coordinates of the quantum hydrogen atom

The optimized geometry of 2 at the CCSD(T)/cc-pVQZ level				
Atom	Number	Coordinates [Bohr]		
		X	Y	Z
C	1	0.000000	0.000000	2.130982
C	2	0.000000	-2.239563	0.731188
C	3	0.000000	2.239563	0.731188
O	4	0.000000	-2.229682	-1.682393
O	5	0.000000	2.229682	-1.682393
H	6	0.000000	0.000000	4.166644
H	7	0.000000	-4.079697	1.658786
H	8	0.000000	4.079697	1.658786
H*	9	0.000000	0.000000	-2.126078

* The coordinates of the quantum hydrogen atom

The averaged geometry of 4				
Atom	Number	Coordinates [Bohr]		
		X	Y	Z
C	1	0.000000	0.000000	4.458367
C	2	2.288822	0.000000	3.124956
C	3	-2.288822	0.000000	3.124956
O	4	2.439951	0.000000	0.711995
O	5	-2.439951	0.000000	0.711995
H	6	0.000000	0.000000	6.497257
H	7	4.077565	0.000000	4.152645
H	8	-4.077565	0.000000	4.152645
Bq*	9	-0.564373	0.000000	0.132820
Bq*	10	0.564373	0.000000	0.132820

* The coordinates of the “ghost atoms” used as the centers of expansion for the electronic basis functions of the quantum hydrogen atom coinciding with the maxima of the ground state protonic orbital.

The averaged geometry of 5				
Atom	Number	Coordinates [Bohr]		
		X	Y	Z
C	1	0.000000	0.000000	4.458367
C	2	2.288822	0.000000	3.124956
C	3	-2.288822	0.000000	3.124956
O	4	-2.439951	0.000000	0.711995
O	5	2.439951	0.000000	0.711995
H	6	0.000000	0.000000	6.497257
H	7	4.077565	0.000000	4.152645
H	8	-4.077565	0.000000	4.152645
Bq*	9	-0.582494	0.000000	0.121241
Bq*	10	0.582494	0.000000	0.121241

* The coordinates of the “ghost atoms” used as the centers of expansion for the electronic basis functions of the quantum hydrogen atom coinciding with the maxima of the excited state protonic orbital.

The regression procedure: Transforming the numerical protonic wavefunctions into the Gaussian-type orbitals

The numerical ground and excited protonic orbitals, obtained by the 3D Numerov method, were fitted by linear combinations of [6s6p6d] Cartesian Gaussian-type shells which were placed on the molecular symmetry plane of the averaged geometry that contains all the clamped nuclei. This is called the xz plane where the x-axis is the C₂ geometrical symmetry axis with respect to the rotation of the clamped nuclei. In the fitting procedure, the protonic orbital is explicitly shown by:

$$\Psi_{ground\ state} = \sum_{i=1}^{15} [c_i \varphi_{\alpha_i}(x_i, y_i, z_i) + c_i \varphi_{\alpha_i}(-x_i, y_i, z_i)],$$

and,

$$\Psi_{excited\ state} = \sum_{i=1}^{15} [c_i \varphi_{\alpha_i}(x_i, y_i, z_i) - c_i \varphi_{\alpha_i}(-x_i, y_i, z_i)],$$

where c_i , α_i and (x_i, y_i, z_i) are the coefficients, exponents and coordinates of the center of i -th *normalized* Gaussian function in these series, respectively. It must be noted that only non-zero contributions, due to the molecular symmetry, were included in the wavefunction expansions and offered in the forthcoming tables of the optimal parameters. The following tables gather the optimized parameters of the protonic orbitals, which were derived after the fitting of the Gaussian expansions to the 3D grid of the protonic wavefunctions.

Regression parameters of the ground state protonic orbital							
Function Number	Shell Number	Function Type	Exponent	Coefficient	Coordinates [Bohr]		
					X	Y	Z
1	1	S	5.92536	-0.667308	0.098133	0.000000	-0.042515
2	2	S	4.90609	0.103662	0.831002	0.000000	-0.082282
3	3	S	5.53872	0.971034	0.256124	0.000000	-0.022740
4	4	Pz	9.99765	-0.025588	0.894294	0.000000	-0.102668
5	5	Pz	5.98643	0.277155	0.488342	0.000000	-0.086228
6	6	Pz	8.71275	-0.067002	0.668808	0.000000	0.221253
7	7	Dxx	6.17956	0.583140	0.559992	0.000000	0.043214
8	7	Dyy	6.17956	-0.405039	0.559992	0.000000	0.043214
9	7	Dzz	6.17956	0.505316	0.559992	0.000000	0.043214
10	8	Dxx	6.97638	0.417660	0.736994	0.000000	0.148422
11	8	Dyy	6.97638	-0.295682	0.736994	0.000000	0.148422
12	8	Dzz	6.97638	0.230332	0.736994	0.000000	0.148422
13	9	Dxx	6.33365	-0.999577	0.649366	0.000000	0.093094
14	9	Dyy	6.33365	0.756131	0.649366	0.000000	0.093094
15	9	Dzz	6.33365	-0.587118	0.649366	0.000000	0.093094

Regression parameters of the excited state protonic orbital							
Function Number	Shell Number	Function Type	Exponent	Coefficient	Coordinates [Bohr]		
					X	Y	Z
1	1	S	7.94753	-0.995443	0.063433	0.000000	-0.199071
2	2	S	8.43716	0.469871	0.967696	0.000000	0.165908
3	3	S	6.71810	0.999654	0.280224	0.000000	-0.116529
4	4	Pz	6.37756	-0.778184	0.720576	0.000000	0.060806
5	5	Pz	7.81809	0.835965	0.545553	0.000000	0.019451
6	6	Pz	7.93854	0.155353	0.834297	0.000000	0.249593
7	7	Dxx	7.17292	0.272671	0.498309	0.000000	0.080944
8	7	Dyy	7.17292	0.310717	0.498309	0.000000	0.080944
9	7	Dzz	7.17292	0.434034	0.498309	0.000000	0.080944
10	8	Dxx	6.66305	-0.207159	0.560419	0.000000	0.028372
11	8	Dyy	6.66305	-0.999654	0.560419	0.000000	0.028372
12	8	Dzz	6.66305	-0.402189	0.560419	0.000000	0.028372
13	9	Dxx	6.30875	-0.468891	0.618625	0.000000	0.067678
14	9	Dyy	6.30875	0.861386	0.618625	0.000000	0.067678
15	9	Dzz	6.30875	0.019168	0.618625	0.000000	0.067678

Table S1- Summary of the ab initio NEO-DFT results.

Method/basis set System	B3LYP-EPC17-1/[cc-pVTZ:10s10p10d]	
	2	1 and 3
<i>Electronic kinetic energy</i>	265.577772	265.554369
<i>Proton's kinetic energy</i>	0.007718	0.007746
<i>Electron-electron potential energy</i>	261.422933	258.206955
<i>Proton-electron potential energy</i>	-13.233539	-12.654149
<i>electron-clamped nuclei potential energy</i>	-949.386639	-943.531760
<i>Proton-clamped nuclei potential energy</i>	12.255060	11.684860
<i>Clamped Nuclei-clamped Nuclei potential energy</i>	156.082444	153.453666
Total energy	-267.274253	-267.278314
Virial ratio	2.006359	2.006463
Method/basis set System	B3LYP/[cc-pVTZ:6s6p6d]	
	4	5
<i>Electronic kinetic energy</i>	265.443959	265.454513
<i>Proton's kinetic energy</i>	0.005092	0.005817
<i>Electron-electron potential energy</i>	258.213390	258.215910
<i>Proton-electron potential energy</i>	-12.401579	-12.396164
<i>electron-clamped nuclei potential energy</i>	-943.513438	-943.531044
<i>Proton-clamped nuclei potential energy</i>	11.709815	11.712679
<i>Clamped Nuclei-clamped Nuclei potential energy</i>	153.388670	153.388670
Total energy	-267.154092	-267.149620
Virial ratio	2.006423	2.006364